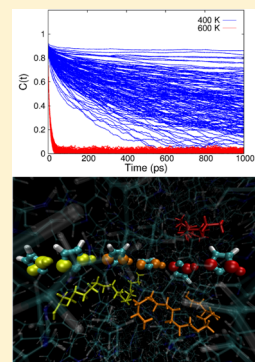


# Simulating Hydrogen-Bond Structure and Dynamics in Glassy Solids Composed of Imidazole Oligomers

Jacob A. Harvey<sup>\*,†</sup> and Scott M. Auerbach<sup>\*,†,‡</sup><sup>†</sup>Department of Chemistry, University of Massachusetts Amherst, Amherst, Massachusetts 01003-9336, United States<sup>‡</sup>Department of Chemical Engineering, University of Massachusetts Amherst, Amherst, Massachusetts 01003-9336, United States**S** Supporting Information

**ABSTRACT:** We simulated structural and dynamical properties of imidazoles tethered to aliphatic backbones to determine how chain length influences the competition between extended hydrogen-bond networks and imidazole reorientation dynamics. We performed molecular dynamics simulations on hypothetical solids using the GAFF Amber force field over the temperature range 300–800 K, for chain lengths varying from monomers to pentamers. We investigated the effect of heterogeneity by simulating monodisperse and polydisperse solids with the same average chain length. We computed hydrogen-bond cluster sizes and percolation ratios; orientational order parameters associated with imidazole rings, tethering linkers, and backbones; and orientational correlation functions for imidazole rings. We found the surprising result that chain-length heterogeneity negligibly affects system density at standard pressure, the fraction of percolating hydrogen-bonded clusters, and the order parameters for backbone, linker, and imidazole ring. Decreasing oligomer chain length from pentamers to shorter chains decreases the tendency to form percolating hydrogen-bond networks while dramatically decreasing imidazole ring reorientation times from a broad range of 100–700 ps for pentamers down to 20 ps for monomers, hence quantifying the competition between hydrogen-bond cluster size and reorientation rate. The computed orientational order parameters suggest the following hierarchy of structural excitations: imidazole ring reorientation in the range 400–500 K, linker motion around 500–600 K, and backbone relaxation at 600–700 K in this model. The question remains for this class of systems which of these motions is crucial for facile proton transport.

**■ INTRODUCTION**

Hydrogen bonding in scaffolded systems is important in many areas of science including self-assembly of organic molecules and biomolecules,<sup>1–3</sup> proton sponges with tunable proton transfer barriers,<sup>4–6</sup> biological proton pumps,<sup>7,8</sup> and anhydrous proton exchange membrane (PEM) fuel cells.<sup>9–11</sup> Amphiprotic groups such as imidazole, which both donate and accept hydrogen bonds, have been widely investigated in PEM materials.<sup>12</sup> Tethering amphiprotic groups to polymeric backbones in PEMs is a strategy for preventing evaporative loss of such groups at elevated temperatures. However, such tethering also constrains dynamical motions thought to be important for facile proton transfer and conduction. Proton transfer in these materials is thought to occur via collective rearrangements of hydrogen bonds known as Grotthuss shuttling,<sup>13</sup> which relies on extended hydrogen-bonding networks. It has been suggested that understanding the structure of the hydrogen-bond network within a material may help infer the materials ability to transport protons.<sup>14,15</sup> After such hydrogen-bond rearrangement, reorientation of amphiprotic groups is required for proton conduction from the anode to the cathode of a fuel cell, i.e., for unidirectional proton motion. It has been suggested that understanding the structure of the hydrogen-bond network within a material may help infer the materials ability to transport protons.<sup>14,15</sup> After such hydrogen-bond rearrangement, reorientation of amphiprotic groups is required for proton conduction from the anode to the cathode of a fuel cell, i.e., for unidirectional proton motion. It has been suggested that understanding the structure of the hydrogen-bond network within a material may help infer the materials ability to transport protons.<sup>14,15</sup> After such hydrogen-bond rearrangement, reorientation of amphiprotic groups is required for proton conduction from the anode to the cathode of a fuel cell, i.e., for unidirectional proton motion. It has been suggested that understanding the structure of the hydrogen-bond network within a material may help infer the materials ability to transport protons.<sup>14,15</sup>

Such a competition has previously been studied in crystalline imidazole;<sup>16,17</sup> here we investigate this competition for imidazoles tethered to aliphatic backbones in glassy, amorphous solids.

The majority of published work on anhydrous PEMs has focused on high-molecular-weight polymers with tethered amphiprotic groups.<sup>9–12,18–21</sup> A few studies on oligomeric systems have, however, been reported; these materials typically involve only mono- or difunctionalized oligomers where amphiprotic groups are separated by relatively long, flexible spacers.<sup>22–26</sup> As such, the effect of varying chain length on hydrogen bonding and reorientation dynamics in multifunctionalized, short-chain oligomers remains poorly known. In previous work, we have shown that solids composed of 5-mers and 10-mers of tethered imidazole exhibit glassy behaviors combining properties of ordered solids with those of traditional liquids.<sup>27</sup> We have also found that these 5-mers and 10-mers produce virtually identical hydrogen-bond cluster sizes,<sup>27</sup> suggesting that, even at these relatively short chain lengths, hydrogen-bond clusters have reached saturation with respect to oligomer length. For this reason, we simulate below the properties of even shorter oligomer lengths to investigate the transition between liquid and glassy regimes. We also study the

Received: January 20, 2014

Revised: June 19, 2014

Published: June 20, 2014

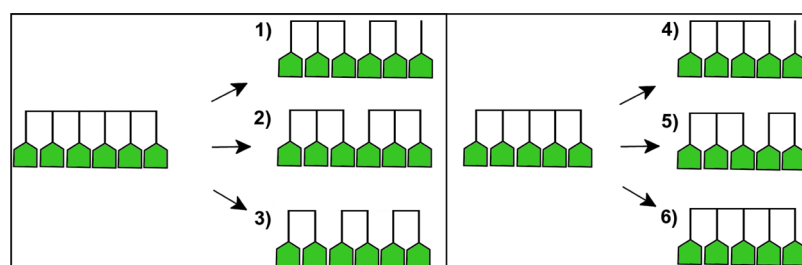


**Figure 1.** Schematic of the different structures used. The  $\langle n \rangle = 2$  (average chain length of 2), trimer, and dimer systems were created using structures 1, 2, and 3, respectively. The  $\langle n \rangle = 3$  system was created using two sheets of structure 4, two of structure 5, and two of structure 6.

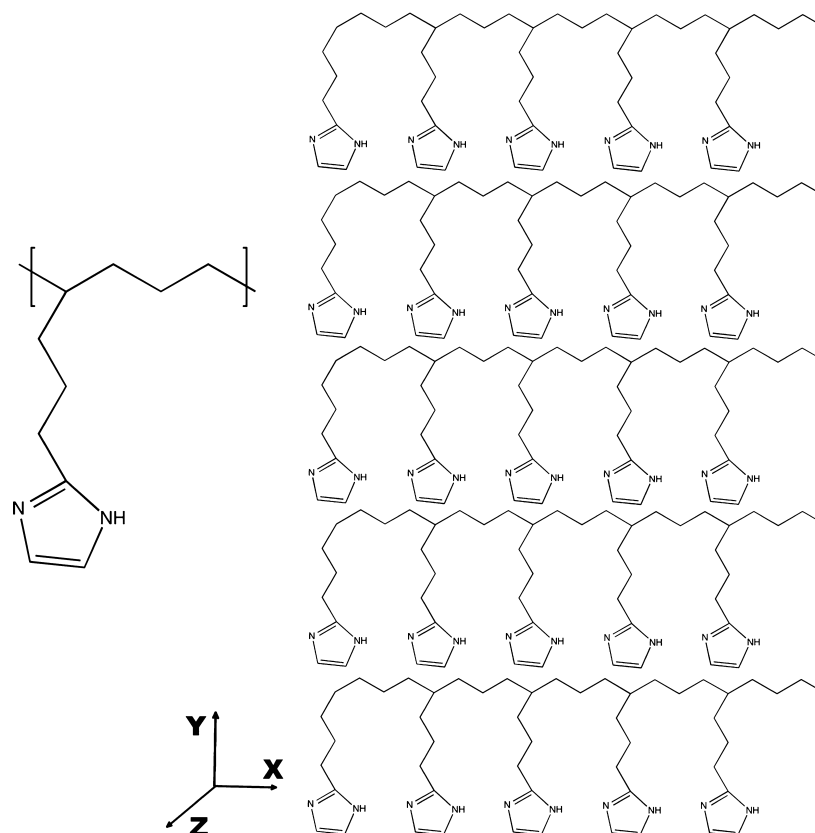


**Figure 2.** (left) Chemical structure of the monomeric repeat unit used. (right) Construction of the two-dimensional sheets. Sheets are stacked in the  $z$  direction.

effect of heterogeneity in chain length, which is likely to arise under realistic synthesis conditions.

Design criteria for making effective PEMs are few; in addition to using protogenic groups with low  $pK_a$  values, polymer chemists often study polymers with low glass-transition temperatures ( $T_g$ ) in hopes that enhanced polymer motion facilitates functional-group reorientation.<sup>11,19,21,28,29</sup> However, it is not obvious that the physics underlying  $T_g$ —which is often associated with the dynamics of polymer chains moving relative to one another<sup>30</sup>—is directly related to functional group reorientation. To investigate this issue, we compute below order parameters associated with reorientation of imidazole rings, tethering linkers, and backbone moieties, to determine if their respective temperature dependencies suggest similar underlying physics or not.

Below we apply molecular dynamics to simulate hydrogen-bond networking and reorientation dynamics of various imidazole oligomers, finding the surprising result that chain-

length heterogeneity has little effect on cluster size. We also find that the onset of glassy behavior occurs for trimeric oligomers, and that there is a hierarchy of excitations with functional-group rotation activating at lower temperatures, linker groups at intermediate temperatures, and backbone relaxation at higher temperatures. We suggest that oligomers, and not polymers, may exhibit optimal trade-offs between extended hydrogen-bond networks and rapid reorientation dynamics for effective PEM materials.

## THEORETICAL METHODS

**Systems.** We modeled molecular solids composed of oligomers of various repeat lengths (see Figure 1), where each oligomer is composed of an aliphatic backbone, tethered imidazoles, and propyl groups linking imidazoles to the backbone (see Figure 2). As shown in Figure 2, each tethered imidazole is attached to its backbone at every fourth backbone carbon; this spacing, along with the propyl linkers, were found

in our previous work<sup>27,31</sup> to allow for extended hydrogen-bonding structures in these materials. We modeled systems composed of oligomers of lengths  $n = 1, 2, 3,$  and  $5$ , where  $n$  is the number of repeat units (i.e., the structure in Figure 2) in each oligomer. The  $n = 1$  (monomer) system is simply a molecular solid composed of heptyl imidazole.<sup>24</sup> For comparison, we also simulated neat liquid imidazole as described below.

We studied the effect of chain-length heterogeneity by comparing results from monodisperse and polydisperse oligomeric solids. Referring to Figure 1, Table 1 indicates

**Table 1. System Composition: Structure Type, Sheet Size, and Number of Sheets**

system	wire type(s)	no. of each wire per sheet	no. of sheets
$\langle n \rangle = 2$	1	5	5
trimers	2	5	5
dimers	3	5	5
$\langle n \rangle = 3$	4	5	2
$\langle n \rangle = 3$	5	5	2
$\langle n \rangle = 3$	6	5	2
pentamers	6	6	5

how each system was constructed. For example, the homogeneous dimer system ( $n = 2$ ) was composed exclusively of structure 3 in Figure 1 (left). Sheets of five “triple dimers” were formed with the imidazoles of one chain proximal to adjacent backbones. Five such sheets were then packed into a three-dimensional material in a way that maximizes  $\pi$ – $\pi$  stacking between adjacent sheets. Figure 2 depicts the monomeric unit used and the chemical structure of the two-dimensional sheets created. Energy minimization at constant pressure (1 atm) was then performed to produce a realistic though hypothetical solid. This system was then heated at constant pressure (1 atm) to 900 K until a convincing melt was obtained, at which point the system was cooled in steps of 100 K back down to 300 K (simulation details given below). For more details regarding the generation of these three-dimensional structures, please see our previous study.<sup>27</sup>

Results from this  $n = 2$  homogeneous dimer system were compared to those from a heterogeneous  $\langle n \rangle = 2$  system (average chain length of 2) composed of 25 copies of structure 1 in Figure 1, i.e., a mix of monomers, dimers, and trimers—formed in sheets, stacked, and annealed as described above. We also studied the comparison between the homogeneous trimer ( $n = 3$ ) and heterogeneous trimer ( $\langle n \rangle = 3$ ) systems. The  $n = 3$  homogeneous trimer was composed of structure 2 in Figure 1, while the  $\langle n \rangle = 3$  heterogeneous trimer system included two sheets each built from structures 4, 5, and 6 in Figure 1 (right). Finally, the pentamer ( $n = 5$ ) system included only structure 6 in Figure 1.

In general, all oligomeric solids studied below contained 150 imidazoles. Our previous study showed that, after annealing, pentameric solids containing 150 and 300 imidazoles (i.e., 30 and 60 pentamers, respectively) exhibit essentially identical hydrogen-bonding properties, indicating that the systems studied below are very likely converged with respect to system size for the properties of interest.

Bulk densities and reorientation time scales of the oligomeric systems were compared to those from neat imidazole liquid. An initial structure of the liquid was generated by heating a crystal structure containing 533 imidazoles until a melt was formed.<sup>27</sup>

Cooling the resulting melt at constant pressure (1 atm) to the desired temperature in the liquid range was performed to produce experimentally comparable densities.

**Simulation Details.** The “generalized AMBER force field” (GAFF<sup>32</sup>) was used with the DL-POLY molecular dynamics code<sup>33</sup> for all simulations. The functional form of GAFF is given by

$$\begin{aligned}
 V(\vec{X}) = & \sum_{b=1}^{n_{\text{bonds}}} \frac{1}{2} k_b (r_b - r_{b0})^2 + \sum_{a=1}^{n_{\text{angles}}} \frac{1}{2} k_a (\theta_a - \theta_{a0})^2 \\
 & + \sum_{t=1}^{n_{\text{torsions}}} \frac{1}{2} V_t [1 + \cos(\omega_t - \gamma_t)] \\
 & + \sum_{i>j}^{N_{\text{atoms}}} \epsilon_{ij} \left[ \left( \frac{r_{ij0}}{r_{ij}} \right)^{12} - 2 \left( \frac{r_{ij0}}{r_{ij}} \right)^6 \right] + \frac{q_i q_j}{4\pi\epsilon_0 r_{ij}} \quad (1)
 \end{aligned}$$

where  $\vec{X}$  is a point in the  $3N_{\text{atoms}}$ -dimensional configuration space. Atomic charges were calculated for the monomer using the B3LYP/6-311G(d,p) model chemistry by fitting point charges to the electrostatic potential using the approach of Kollman and co-workers<sup>34,35</sup> as implemented in Gaussian 09.<sup>36</sup> The monomer charge set was applied to each monomer in each chain of the system. In our previous work, we found that the B3LYP/6-311G(d,p) model chemistry converged hydrogen-bonding properties reasonably well with respect to basis set and level of theory,<sup>31</sup> and that GAFF reproduced B3LYP/6-311G(d,p) results for imidazole hydrogen-bond strengths and rotational barriers.<sup>27</sup> All simulations reported herein were performed using three-dimensional periodic boundary conditions with a 10 Å cutoff for short-range potentials and the Ewald summation for Coulombic interactions. Each molecular dynamics simulation was performed with a 1 fs time step.

As described above, initial conditions for production runs were obtained by heating hypothetical ordered solids up to 900 K, followed by sequential cooling runs producing disordered solids at target temperatures between 300 and 800 K. Because GAFF is not a reactive force field, we do not observe chemical decomposition as might be expected in actual experiments at such elevated temperatures. All simulations were performed in the  $NpT$  ensemble because of the need to predict densities for these hypothetical solids, by coupling a Nosé–Hoover thermostat (1 ps relaxation time) to a barostat (2 ps relaxation time).<sup>37</sup> All simulations were performed in orthorhombic simulation cells; see Tables S1 and S2 in the Supporting Information for the resulting mean lattice parameters computed herein.

An equilibrium snapshot of the  $NpT$  ensemble simulations, with the corresponding mean lattice parameters, was used to start  $NVE$  simulations of the pentamer system at each temperature. These simulations were used to examine the robustness of the force field at high temperatures and the effect of a thermostat/barostat on calculated dynamical reorientation time scales as discussed below. Temperature distributions at 800 K were calculated for the  $NVE$  and  $NpT$  simulations, which are shown in Figure S1 (Supporting Information). A shift in the peak from 796 to 803 K is observed when moving from the  $NpT$  ensemble to the  $NVE$  ensemble. This shift is much smaller than our nominal shifts in temperature for each system (100 K). Moreover, the drift in temperature remains negligible in the  $NVE$  ensemble ( $-1.8 \times 10^{-2}$  K/ns) and is only a marginal increase from the  $NpT$  simulations ( $-1.4 \times 10^{-2}$  K/ns).

Simulations were initiated from equilibrium snapshots taken from the adjacent higher temperature. Each simulation involved a 1 ns equilibration period and a 5 ns period of data collection to harvest statistics on hydrogen-bonding structure and dynamics; these times were found sufficient for gathering statistics for the properties of interest. Production simulations were carried out on our beowulf cluster using 24 2.53 GHz processors (three nodes), requiring roughly 45 CPU hours per temperature.

**Percolation Ratios.** As discussed in the Introduction, the basic purpose of this article is to study the competition between the formation of extended hydrogen-bonding networks on the one hand and rapid functional group reorientation dynamics on the other hand. In this section, we describe our approach for characterizing the collective structure of the hydrogen-bond networks that arise in our simulations. A hydrogen-bond network can be viewed as a three-dimensional cluster, albeit one with a relatively short lifetime. Clusters may be characterized through a connectivity matrix as described in our previous work;<sup>27</sup> here we give a brief review of our approach to hydrogen-bond cluster statistics.

The connectivity matrix indicates the connectivity between imidazoles as follows:<sup>38</sup>

$$C_{ij} = \begin{cases} 1 & \text{if imidazoles } i \text{ and } j \text{ are connected by a} \\ & \text{single hydrogen-bond network} \\ 0 & \text{otherwise} \end{cases}$$

The full connectivity matrix can be decomposed into two terms according to

$$C_{ij} = C_{ij}^{\text{direct}} + C_{ij}^{\text{indirect}} \quad (2)$$

The directly connected matrix elements equal unity if imidazoles  $i$  and  $j$  form a hydrogen bond together. Hydrogen bonds are counted when an intermolecular  $\text{NH}\cdots\text{N}$  distance is less than 2.5 Å. This cutoff distance is standard and was used in our previous study;<sup>27</sup> our present cluster statistics were found to be relatively insensitive to small changes to this cutoff value (data not shown). The direct portion of the connectivity matrix is determined by a double loop over all imidazoles. The indirectly connected matrix can be determined using the following relationship:

$$\text{If } C_{ij} = 1 \text{ and } C_{jk} = 1, \text{ then } C_{ik} = 1$$

In practice, this involves comparing the column of imidazole  $i$  to the column of imidazole  $j$ . If the two columns share a nonzero element, they are indirectly bound and the two columns are replaced with the union of the two. In addition, the two imidazoles are assigned a common cluster label. This process is continued until all imidazoles have been assigned a cluster label, hence determining the full connectivity matrix.

Below we report what is perhaps the most collective structural property of a simulated hydrogen-bond network, namely, its percolation ratio. This is defined<sup>39</sup> as the fraction of all imidazole functional groups that participate in clusters extending from one edge of the simulation cell to another. In the present study, as in our previous work, we identified edge imidazoles somewhat arbitrarily as rings where at least three non-hydrogen atoms are within 4.5 Å of the edge of the simulation cell. This distance roughly represents the kinetic diameter of an imidazole.

In our previous work, the extent of hydrogen-bond percolation was presented as a percent of the maximum number of possible percolating pathways. This maximum value was taken somewhat arbitrarily to be the number of hydrogen-bonding chains in the initially formed, ordered solids before annealing (either 25 chains for structures 1–3 in Table 1 or 30 chains for structures 4–6). In addition to the arbitrariness of this normalization, simply counting percolating pathways treats long and short pathways equally, and hence does not reflect the *volume fraction* of amphiprotic groups participating in extended hydrogen bonding. For these reasons, we focus below on reorienting percolation ratios.

**Reorientation Dynamics.** The reorientation dynamics of imidazole rings were probed by computing the orientational autocorrelation function given by

$$\tilde{C}(t) = \langle N(0) \cdot N(t) \rangle - \langle N \rangle \cdot \langle N \rangle \quad (3)$$

where  $C(t)$  is the correlation function (not to be confused with the connectivity matrix) and  $N(t)$  is the unit vector normal to the plane of an imidazole at time  $t$ . Below we study orientational dynamics in glassy solids and isotropic liquids. In either case, if we were to run molecular dynamics for a sufficiently long time, we would find that the orientational order parameter  $|\langle N \rangle|$  would vanish within statistical precision. However, in our 5 ns simulations, we find that this order parameter contains useful information on the transition from glass to liquid with increasing temperature, or from liquid to glass with increasing oligomer chain length. As such, we view this order parameter as a quasi-structural property of the system, and study this separately from the unshifted orientational autocorrelation function, given by

$$C(t) = \langle N(0) \cdot N(t) \rangle \quad (4)$$

We also computed orientational order parameters for linker motions and backbone fluctuations using the unit vectors shown in Figure 3. A study of the temperature dependencies of these three order parameters allows us to investigate the hierarchy of motions present in these glassy solids.

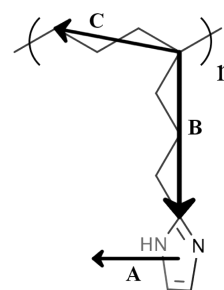


**Figure 3.** Vectors used to compute the orientational order parameter for the (A) imidazole rings, (B) linker, and (C) backbone.

The unshifted autocorrelation function was found to exhibit a biexponential form— $C(t) = b + ae^{-t/\tau_1} + (1 - a)e^{-t/\tau_2}$ —especially for glassy systems. We used this form to fit all of our correlation functions. The longer time scale ( $\tau_2$ ) was extracted as the reorientation time scale of each imidazole. The shorter time scale ( $\tau_1$ ) is associated with rapid, hindered vibrations (i.e., librations) of each ring.<sup>40</sup> Autocorrelation functions were computed and reported for each imidazole separately, which yields a distribution of reorientation time scales. Glassy systems exhibited a relatively broad distribution of reorientation times,

while liquids gave a rather narrow distribution of such times. In contrast, the orientational order parameter discussed above is reported below as an average over all relevant moieties in the system.

Distributions of the reorientation time scales for  $NpT$  runs are compared with the analog  $NVE$  run in Figure S3 (Supporting Information) for the pentamer system at 400–700 K. Our results show very little change in the dynamical quantities when using a thermostat and barostat. This suggests that the effect of the thermostat/barostat is mild and that we can draw quantitative conclusions from our  $NpT$  simulations.

## RESULTS AND DISCUSSION

Here we report system density, percolation ratios, orientational order parameters, and orientational correlation functions of the oligomeric, glassy solids studied herein.

**Density Equation of State.** The temperature dependence of density serves as a quasi-macroscopic measure of the plausibility and behavior of our simulations. We show the density of all systems in Figure 4 as a function of temperature,

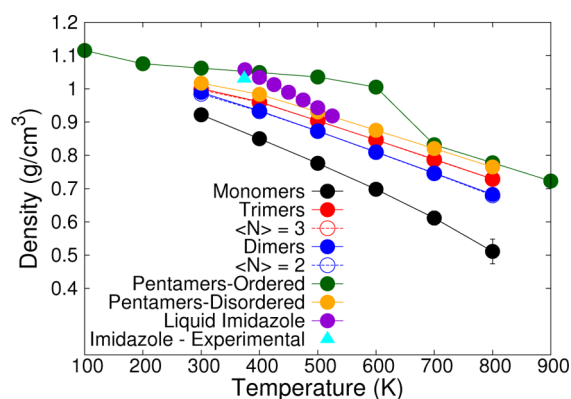


**Figure 4.** Computed density of all systems over the relevant range of temperatures. Heterogeneous systems are shown as open circles; these were found to give densities that are statistically equivalent to their homogeneous counterparts.

all at a target pressure of 1 atm. We observe in Figure 4 that the density is predicted to increase with increasing oligomer chain length, possibly because of better packing with longer chains. The simulated density of neat liquid imidazole is also shown in Figure 4 over the temperature range 380–520 K, in the liquid region of the phase diagram for imidazole at 1 atm. Our simulation results compare very well with an experimental density value at the lower end of this temperature range,<sup>41</sup> which speaks to the validity of our simulation approach and models. Interestingly, the density of neat liquid imidazole at 380 K is at the high end of our computed densities, and is close to that for the ordered pentameric solid. We speculate that the unconstrained fluctuations in the liquid produce high density, as does the excellent packing in the ordered solid. We also observe in Figure 4 that homogeneous (closed circles) and heterogeneous systems (open circles) exhibit statistically equivalent densities. It remains to be seen whether these exhibit similar or different hydrogen-bonding properties.

**Percolation Ratios.** Figure 5 shows the results from our computational study of percolation ratios. All oligomer chain lengths were found to produce nonzero percolation ratios, even at the relatively high temperatures in the melt transition regime (600–700 K) suggested in Figure 4. Increasing oligomer chain

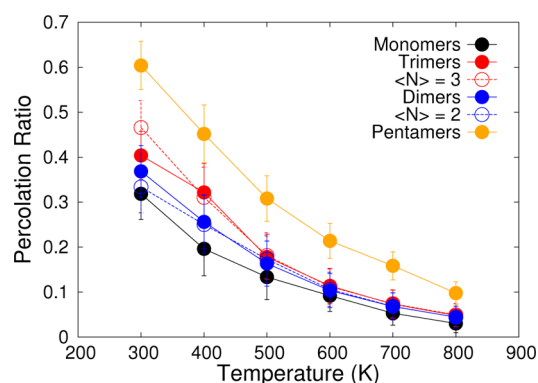


**Figure 5.** Percolation ratio as a function of temperature. The percolation ratio is the fraction of imidazoles in percolating pathways. Heterogeneous (open circles) and homogeneous (closed circles) systems show essentially identical percolation ratios.

length was found to increase the percolation ratio for all temperatures studied, consistent with the notion that adding covalent constraints facilitates extended hydrogen bonding. At 400 K, in the desired high-temperature region of hydrogen fuel cells, the percolation ratio scales linearly with oligomer chain length, while at higher temperatures the monomer, dimer, and trimer percolation ratios take similar values which are significantly lower than those for pentamers. As with the system density in Figure 4, heterogeneity of oligomer chain length seems to produce negligible effects on the percolation ratio except at the lowest temperature (100 K), which may be influenced by some statistical noise. The negligible effect of chain-length heterogeneity suggests that synthetic routes for making these or related oligomers can allow for polydispersity in the oligomeric products. This negligible effect also suggests that mean-field theories may describe some aspects of the structure and dynamics of these oligomeric systems.<sup>42</sup>

We now focus on interpreting the absolute values of the percolation ratios in Figure 5. At 300 K, the pentamer system exhibits a mean percolation ratio of approximately 0.6, indicating that on average 90 out of 150 total imidazoles participate in percolating pathways. To place this value in perspective, we note from our previously published work<sup>27</sup> that the mean hydrogen-bond cluster size for pentamers at 300 K is  $4.7 \pm 0.6$  (see Figure S2 in the Supporting Information for mean cluster sizes for all systems studied herein), and that pentamers exhibit roughly 6 percolating pathways at 300 K, which amounts to 20% of the 30 percolating paths in the initial ordered state. As such, although the mean hydrogen-bonded cluster contains 5 imidazoles, a typical percolating pathway contains  $90/6 = 15$  imidazoles. This analysis suggests that, for pentamers at 300 K, the percolating hydrogen-bond networks in our simulations likely represent rather tortuous pathways. The same analysis at 400 K gives about 69 imidazoles in roughly 3 percolating pathways, or about 23 imidazoles per pathway. This finding of tortuous hydrogen-bonding pathways thus appears to hold for a range of relevant temperatures.

**Orientational Randomization and Structural Excitations.** The temperature dependencies of the orientational order parameters for each structural element—imidazole ring, linker group, and backbone segment—are shown below in Figure 6. For each structural element, increasing the oligomer chain length increases the associated order parameter at a given temperature, as well as the order-parameter fluctuations as measured by the standard deviation shown as error bars in

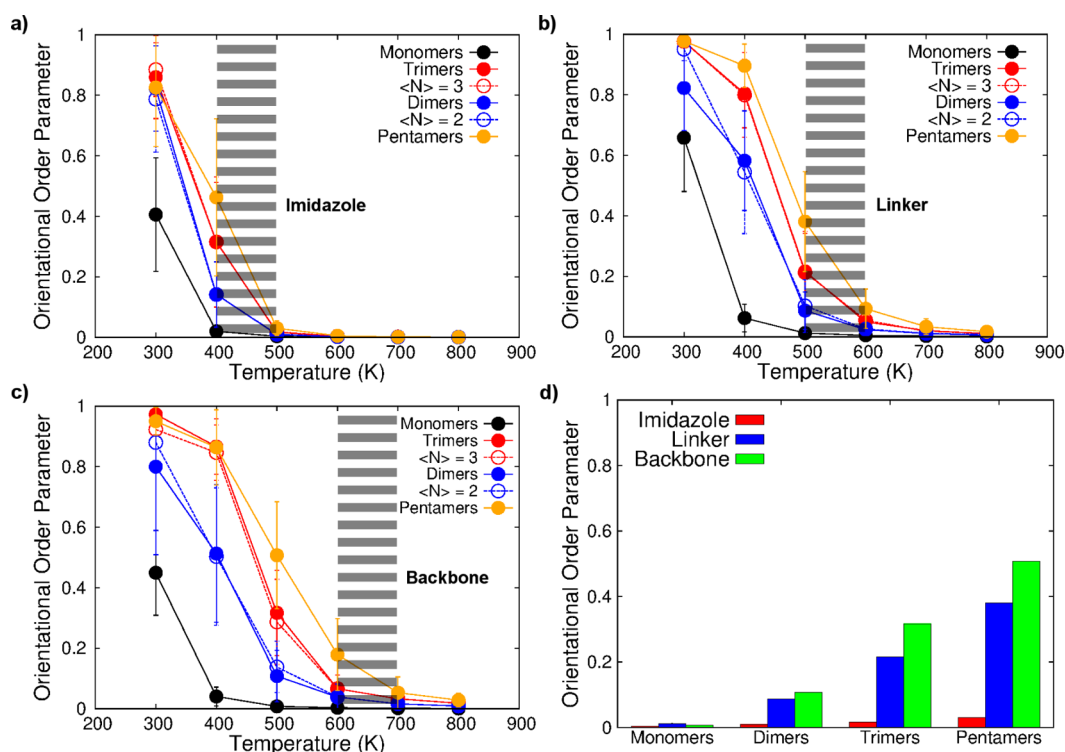


**Figure 6.** Orientational order parameter for (a) imidazoles, (b) linkers, (c) backbone segments, and (d) all three orientational order parameters for various chain lengths at 500 K.

Figure 6. As with our previous results on density and percolation ratio, chain-length heterogeneity has little impact on the orientational order parameters in Figure 6. We note that relatively large standard deviations, as seen, e.g., for imidazole rings (Figure 6a) in the pentamers at 400 K, are characteristic of a wide diversity of environments frozen into a glassy oligomeric solid. In this case, some imidazole rings fluctuate in approximately fixed (i.e., quenched) environments that allow for nearly complete orientational randomization on the simulation time scale (5 ns), while other imidazoles fluctuate in very different quenched environments that essentially trap the orientation of each ring.

The same observation of glassy behavior applies to linker groups (e.g., pentamers at 500 K in Figure 6b) and backbone segments (e.g., pentamers at 500 K in Figure 6c). In fact, one observes in Figure 6 a hierarchy of structural excitations with the following: (i) imidazole-ring rotation becoming activated in the 400–500 K range (cross-hatching in Figure 6a), (ii) linker-group motion activating in the 500–600 K range, and (iii) backbone segment activation in the 600–700 K range. Figure 6d shows all order parameters at 500 K, indicating that at this temperature imidazoles in all the systems studied herein exhibit near-complete orientational randomization, while the linkers and backbones show very similar, partial randomization.

The backbone order-parameter transition correlates with the glass transition of polymers,<sup>30</sup> which is often assumed to be an important parameter for designing PEMs with high proton conductivities.<sup>19,21,28,29</sup> In particular, it is often assumed that polymers with lower glass-transition temperatures ( $T_g$ ) exhibit the kinds of fluid-like motions that promote facile proton transfer and conduction.<sup>19,21,28,29</sup> On the other hand, amphiprotic functional group reorientation is often assumed to be the rate-limiting step in Grotthuss shuttling.<sup>12</sup> The result in Figure 6—distinguishing the temperature ranges and hence

the physics underlying the dynamics of functional group and backbone motion—suggests the possibility that designing PEMs by minimizing  $T_g$  may *not* be the most useful criterion for generating high conductivities. Future work directly simulating proton transport in glassy oligomeric solids is needed to shed light on this question.

**Reorientation Dynamics.** Orientational correlation functions (OCFs) were calculated for each individual imidazole and plotted in Figure 7. Reporting OCFs for each molecule separately, instead of averaging over molecules to yield a single system correlation function, preserves information about the distribution of environments that may be present in glassy oligomeric solids. Figure 7a shows that reorientational time scales at 400 K increase with increasing chain length from monomer to trimer to pentamer, and that the pattern of monomer OCFs is dramatically different from trimer and pentamer OCFs. While all these OCFs were successfully fitted to biexponential functions, the distribution of monomer OCFs is much narrower, characteristic of liquid-like behavior, while trimer and pentamer OCFs in Figure 7a reflect broad distributions of environments characteristic of glasses. At a sufficiently high temperature characteristic of each oligomer chain length, the glass transforms to a liquid as shown for trimers in Figure 7b, which shows a quite narrow distribution of OCFs at 600 K.

As discussed above, each OCF was fitted to a biexponential function of the form  $C(t) = b + ae^{-t/\tau_1} + (1 - a)e^{-t/\tau_2}$ , and  $\tau_2$  was extracted as the reorientation time scale for each imidazole. We constructed histograms of the reorientation time scales as shown for 400 K in Figure 8, including the relaxation time for neat imidazole liquid for comparison. This shows clearly how reorientation time scales increase with increasing chain length, although, for the glassy systems at 400 K, average time scales are less meaningful because of the remarkable breadth in

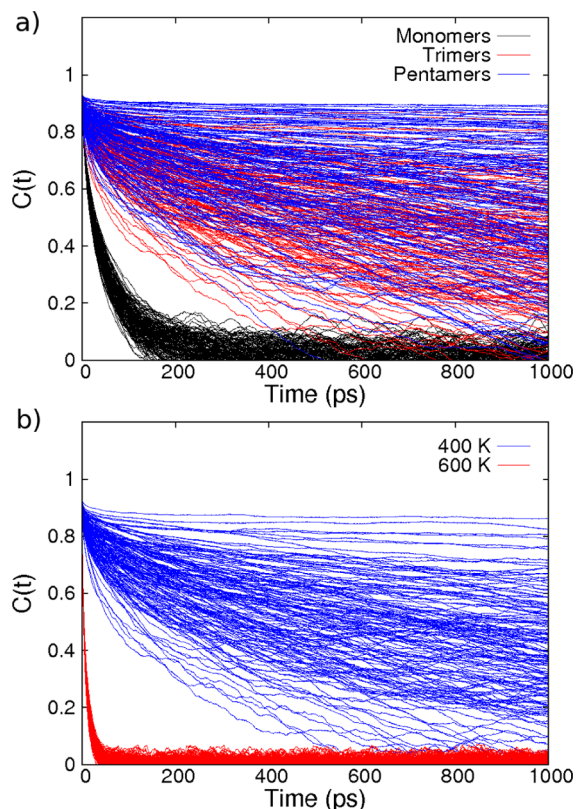


**Figure 7.** Orientational correlation functions of imidazoles for (a) monomers (black), trimers (red), and pentamers (blue) all at 400 K and (b) trimers at 400 and 600 K.

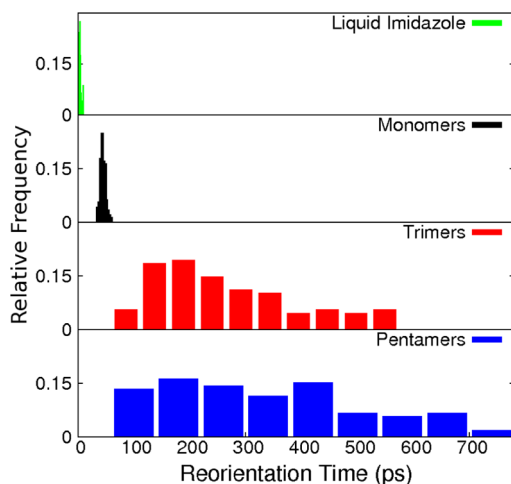


**Figure 8.** Distributions of reorientation time scales for imidazole neat liquid (green), monomers (black), trimers (red), and pentamers (blue) all at 400 K.

relaxation times, especially for pentamers. Figure 8 does provide an interesting quantitative insight. In particular, the relaxation time distribution for neat imidazole is peaked at 3.5 ps, while that for the monomer is peaked at 43 ps, representing more than an order-of-magnitude increase. This increase closely mirrors the 10-fold decrease in experimental proton conductivity of the monomer system relative to the liquid.<sup>24,43</sup> This analysis is consistent with the conventional wisdom that the main effect of tethering on conductivity is to increase the reorientation time scale of amphoteric functional groups.

## SUMMARY AND CONCLUDING REMARKS

We have modeled systems of imidazoles tethered to oligomeric backbones to probe the competition between extended hydrogen-bond networks and rapid reorientation dynamics. The chain length of each oligomer was varied from monomers to dimers, trimers, and pentamers. We used the DL-POLY molecular dynamics code with the generalized AMBER force field to simulate the structure and dynamics of materials composed of collections of such oligomers. These materials were found to exhibit glassy solid behavior at low temperatures and liquid-like properties at higher temperatures, with transition temperatures depending on oligomer chain length. Heterogeneous systems with an average chain length of two and three were studied which, when compared to corresponding homogeneous systems composed solely of dimers and trimers, respectively, probe effects of heterogeneity on hydrogen-bonding networks and orientational randomization. Systems with ordered initial conditions were heated to 900 K, producing disordered liquids which were then cooled sequentially to 300 K in 100 K increments. Global hydrogen-bonding networks were probed by computing percolation ratios, i.e., the fractions of imidazoles participating in hydrogen-bonding pathways that percolate across the simulation cell. Orientational randomization of three structural elements—imidazole ring, linker group, and backbone segment—were studied by computing order parameters based on the corresponding vectors. Orientational correlation functions (OCFs) were calculated for each imidazole, from which distributions of reorientation time scales were extracted.

Increasing oligomer chain length increases percolation ratios by factors of 2–3, hence producing more extended hydrogen-bonding networks, but also increases reorientational time scales of imidazoles by an order of magnitude from monomers to pentamers. We found the surprising result that heterogeneity in oligomer chain length produces no discernible effect in system density, percolation ratio, or orientational randomization of imidazole, linker, or backbone. This finding suggests the practical fact that precise synthetic control over chain length is relatively unimportant for these systems. We observed a hierarchy of structural excitations involving imidazole orientational randomization around 400–500 K, linker-group motion around 500–600 K, and backbone segment activation around 600–700 K. Shorter chains achieve liquid-like dynamics and full orientational randomization at lower temperatures than those of longer chains, with dimers fully activating around 500 K, trimers around 600 K, and pentamers around 700 K.

In general, we observe a clear trade-off between extended hydrogen-bond network formation and rapid orientational dynamics of amphoteric functional groups. Determining how to tune this competition to maximize proton conductivity in the resulting materials remains one of the grand challenges of this field. One might surmise, when considering proton conductivities across several materials, that proton conductivity correlates with percolation ratio, and anticorrelates with the orientational order parameter of the amphoteric functional group. In a forthcoming publication, we will test this idea by simulating proton transfer and diffusion in tethered oligomeric systems such as those studied herein. In any event, we suggest that considering amphoteric functional groups tethered to short-chain oligomers, instead of tethering to polymers, presents an exciting class of targets for designing next-generation PEMs.

## ■ ASSOCIATED CONTENT

### Supporting Information

NVE temperature distributions, mean hydrogen-bond cluster sizes, reorientation time scale distributions, and mean simulation cell lattice parameters for all systems studied. This material is available free of charge via the Internet at <http://pubs.acs.org>.

## ■ AUTHOR INFORMATION

### Corresponding Authors

\*E-mail: jaharvey@chem.umass.edu.

\*E-mail: auerbach@chem.umass.edu.

### Notes

The authors declare no competing financial interest.

## ■ ACKNOWLEDGMENTS

This material is based upon work supported by, or in part by, the U.S. Army Research Laboratory and the U.S. Army Research Office under grant number 54635CH. We also thank Profs. D. Venkataraman, J. Fermann, and M. Tuominen at UMass Amherst for fruitful discussions on proton transport.

## ■ REFERENCES

- (1) Bladon, P.; Griffin, A. Self-Assembly in Living Nematics. *Macromolecules* **1993**, *26*, 6604–6610.
- (2) Zhao, Y.; Stejskal, J.; Wang, J. Towards Directional Assembly of Hierarchical Structures: Aniline Oligomers as the Model Precursors. *Nanoscale* **2013**, *5*, 2620–2626.
- (3) Shih, R.; Lu, C.; Kuo, S.; Chang, F. Hydrogen Bond-Mediated Self-Assembly of Polyhedral Oligomeric Silsesquioxane-Based Supramolecules. *J. Phys. Chem. C* **2010**, *114*, 12855–12862.
- (4) Schwesinger, R.; Missfeldt, M.; Peters, K.; Bonschering, H.; Novel, Very Strongly Basic, Pentacyclic “Proton Sponges” With Vinamidine Structure. *Angew. Chem., Int. Ed.* **1987**, *26*, 1165–1167.
- (5) Verkade, J. Atranes: New Examples With Unexpected Properties. *Acc. Chem. Res.* **1993**, *26*, 483–489.
- (6) Verkade, J. Main Group Atranes: Chemical and Structural Features. *Coord. Chem. Rev.* **1994**, *137*, 233–295.
- (7) Heberle, J. Proton Transfer Reactions Across Bacteriorhodopsin and Along the Membrane. *Biochim. Biophys. Acta* **2000**, *1458*, 135–147.
- (8) Peng, Y.; Voth, G. Expanding the View of Proton Pumping in Cytochrome *C* Oxidase Through Computer simulation. *Biochim. Biophys. Acta* **2012**, *1817*, 518–525.
- (9) Scharfenberger, G.; Meyer, W.; Wegner, G.; Schuster, M.; Kreuer, K.; Maier, J. Anhydrous Polymeric Proton Conductors Based on Imidazole Functionalized Polysiloxane. *Fuel Cells* **2006**, 237–250.
- (10) Herz, H.; Kreuer, K.; Maier, J.; Scharfenberger, G.; Schuster, M.; Meyer, W. New Fully Polymeric Proton Solvents With High Proton Mobility. *Electrochim. Acta* **2003**, *48*, 2165–2171.
- (11) Granados-Focil, S.; Woudenberg, R.; Yavuzcetin, O.; Tuominen, M.; Coughlin, E. Water-Free Proton-Conduction Polysiloxanes: A Study on the Effect of Heterocycle Structure. *Macromolecules* **2007**, *40*, 8708–8713.
- (12) Kreuer, K.; Paddison, S.; Spohr, E.; Schuster, M. Transport in Proton Conductors for Fuel-Cell Applications: Simulations, Elementary Reactions, and Phenomenology. *Chem. Rev.* **2004**, *104*, 4637–4678.
- (13) de Grotthuss, C. *Ann. Chim.* **1806**, LVVII, 54–73.
- (14) Cavalcanti, W.; Portaluppi, D.; Joswig, J.-O. Preconditioning Immobilized Imidazole Arrays for Optimal Proton-Transfer Feasibility. *J. Chem. Phys.* **2010**, *133*, 104703–104709.
- (15) Roy, S.; Ataul, T.; Müller-Plathe, F. Molecular Dynamics Simulations of Heptyl Phosphonic Acid: A Potential Polymer Component for Fuel Cell Polymer Membrane. *J. Phys. Chem. B* **2008**, *112*, 7403–7409.
- (16) Münch, W.; Kreuer, K.; Silvestri, W.; Maier, J.; Seifert, G. The Diffusion Mechanism of an Excess Proton in Imidazole Molecular Chains: First Results of an *Ab initio* Molecular Dynamics Study. *Solid State Ionics* **2001**, *145*, 437–443.
- (17) Iannuzzi, M.; Parrinello, M. Proton Transfer in Heterocycle Crystals. *Phys. Rev. Lett.* **2004**, *93*, 1–4.
- (18) Akbey, U.; Granados-Focil, S.; Coughlin, E.; Graf, R.; Spiess, H. <sup>1</sup>H Solid-State NMR Investigation of Structure and Dynamics of Anhydrous Proton Conducting Triazole-Functionalized Siloxane Polymers. *J. Phys. Chem. B* **2009**, *113*, 9151–9160.
- (19) Martwiset, S.; Woudenberg, R.; Granados-Focil, S.; Yavuzcetin, O.; Tuominen, M.; Coughlin, E. Intrinsically Conducting Polymers and Copolymers Containing Triazole Moieties. *Solid State Ionics* **2007**, *178*, 1398–1403.
- (20) Nagamani, C.; Versek, C.; Thorn, M.; Tuominen, M.; Thayumanavan, S. Proton Conduction in 1H-1,2,3-Triazole Polymers: Imidazole-Like or Pyrazole-Like. *J. Polym. Sci.* **2010**, *48*, 1851–1858.
- (21) Nagamani, C.; Viswanathan, U.; Versek, C.; Tuominen, M.; Auerbach, S.; Thyumanavan, S. Importance of Dynamic Hydrogen Bonds and Reorientation Barriers in Proton Transport. *Chem. Commun.* **2011**, *47*, 6638–6640.
- (22) Schuster, M.; Meyer, W.; Wegner, G.; Herz, H.; Ise, M.; Schuster, M.; Kreuer, K.; Maier, J. Proton Mobility in Oligomer-Bound Proton Solvents: Imidazole Immobilization via Flexible Spaces. *Solid State Ionics* **2001**, *145*, 85–92.
- (23) Schuster, M.; Meyer, W.; Schuster, M.; Kreuer, K. Toward a New Type of Anhydrous Organic Proton Conductor Based on Immobilized Imidazole. *Chem. Mater.* **2004**, *16*, 329–337.
- (24) Schuster, M.; Rager, T.; Noda, A.; Kreuer, K.; Maier, J. About the Choice of the Protogenic Group in PEM Separator Materials for Intermediate Temperature, Low Humidity Operation: A Critical Comparison of Sulfonic Acid, Phosphonic Acid and Imidazole Functionalized Model Compounds. *Fuel Cells* **2005**, *5*, 355–365.
- (25) Steininger, H.; Schuster, M.; Kreuer, K.; Kaltbeitzel, A.; Bingöl, B.; Meyer, W.; Schauff, S.; Brunklaus, G.; Maier, J.; Spiess, H. Intermediate Temperature Proton Conductors for PEM Fuel Cells Based on Phosphonic Acid as Protogenic Group: A Progress Report. *Phys. Chem. Chem. Phys.* **2007**, *9*, 1764–1773.
- (26) Paddison, S.; Kreuer, K.; Maier, J. About the Choice of the Protogenic Group in Polymer Electrolyte Membranes: *Ab initio* Modelling of Sulfonic Acid, Phosphonic Acid, and Imidazole Functionalized Alkanes. *Phys. Chem. Chem. Phys.* **2006**, *8*, 4530–4542.
- (27) Harvey, J.; Basak, D.; Venkataraman, D.; Auerbach, S. Simulating Hydrogen-Bond Clustering and Phase Behaviour of Imidazole Oligomers. *Mol. Phys.* **2012**, *110*, 957–966.
- (28) Persson, J.; Jannasch, P. Intrinsically Proton-Conducting Benzimidazole Units Tethered to Polysiloxanes. *Macromolecules* **2005**, *38*, 3283–3289.
- (29) Martwiset, S.; Yavuzcetin, O.; Thorn, M.; Versek, C.; Tuominen, M.; Coughlin, E. Proton Conducting Polymers Containing 1H-1,2,3-Triazole Moieties. *J. Polym. Sci., Part A: Polym. Chem.* **2009**, *47*, 188–196.
- (30) Cowie, J.; Arrighi, V. *Polymers: Chemistry and Physics of Modern Materials*; CRC Press: Boca Raton, FL, 2008.
- (31) Viswanathan, U.; Basak, D.; Venkataraman, D.; Fermann, J.; Auerbach, S. Modeling Energy Landscapes of Proton Motion in Nonaqueous, Tethered Proton Wires. *J. Phys. Chem. A* **2011**, *115*, 5423–5434.
- (32) Wang, J.; Wolf, R.; Caldwell, J.; Kollman, P.; Case, D. Development and Testing of a General Amber Force Field. *J. Comput. Chem.* **2004**, *25*, 1157–1174.
- (33) Smith, W.; Forester, T. DL\_Poly\_2.0: A General-Purpose Parallel Molecular Dynamics Simulation Package. *J. Mol. Graphics* **1996**, *14*, 136–141.
- (34) Besler, B.; Merz, K., Jr.; Kollman, P. Atomic Charges Derived From Semiempirical Methods. *J. Comput. Chem.* **1990**, *11*, 431–439.
- (35) Singh, U.; Kollman, P. An Approach to Computing Electrostatic Charges for Molecules. *J. Comput. Chem.* **1984**, *5*, 129–145.

(36) Frisch, M. J.; Trucks, G. W.; Schlegel, H. B.; Scuseria, G. E.; Robb, M. A.; Cheeseman, J. R.; Scalmani, G.; Barone, V.; Mennucci, B.; Petersson, G. A.; et al. *Gaussian 09*, revision D.01; Gaussian, Inc.: Wallingford, CT, 2009.

(37) Melchionna, S.; Ciccotti, G.; Holian, B. Hoover NPT Dynamics for Systems Varying in Shape. *Mol. Phys.* **1993**, *78*, 533–544.

(38) Sevick, E.; Monson, P.; Ottino, J. Monte Carlo Calculations of Cluster Statistics in Continuum Models of Composite Morphology. *J. Chem. Phys.* **1988**, *88*, 1198–1206.

(39) Lee, C.; Pao, C.; Chu, C. Multiscale Molecular Simulations of the Nanoscale Morphologies of P3HT:PCBM Blends for Bulk Heterojunction Organic Photovoltaic Cells. *Energy Environ. Sci.* **2011**, *4*, 4124–4132.

(40) Spohr, E.; Commer, P.; Kornyshev, A. Enhancing Proton Mobility in Polymer Electrolyte Membranes: Lessons From Molecular Dynamics Simulations. *J. Phys. Chem. B* **2002**, *106*, 10560–10569.

(41) Lide, D. *Physical Constants of Organic Compounds*, In *Handbook of Chemistry and Physics*; CRC Press: Boca Raton, FL, 2007.

(42) Monson, P. Mean Field Kinetic Theory for a Lattice Gas Model of Fluids Confined in Porous Materials. *J. Chem. Phys.* **2008**, *128*, 084701–084710.

(43) Kreuer, K.; Fuchs, A.; Ise, M.; Spaeth, M.; Maier, J. Imidazole and Pyrazole-Based Proton Conducting Polymers and Liquids. *J. Electrochim. Acta* **1998**, *43*, 1281–1288.